

Fast BE Calculation of Acoustic Radiation from Vibrating Structures by Mortar Coupling

L. Gaul¹, M. Fischer¹

Summary

A mortar algorithm for the simulation of acoustic-structure interaction is presented that allows the coupling of non-conforming FE and BE discretizations. Computing cost and memory requirements can be reduced by employing the fast multipole BEM for the acoustic domain.

Acoustic-Structure Interaction

A structure is fully submerged in an acoustic fluid as displayed in Fig. 1 and is modeled as a thin Kirchhoff plate on the interaction boundary Γ^{int} . The out-of-plane displacement is denoted by w , the loading $f = f^0 + f^e$ consists of surface forces due to the acoustic field f^0 and externally applied forces f^e . The time-harmonic pressure p in the acoustic field Ω_f is governed by the Helmholtz equation $\Delta p + \kappa^2 p = 0$ with the circular wavenumber $\kappa = \omega/c_0$. The acoustic flux on the boundary is defined as $q = \partial p / \partial \vec{n}_f$. For simplicity of presentation, the boundary $\partial\Omega_f = \Gamma = \Gamma^{\text{int}} \cup \Gamma^{\text{N}}$ is composed of acoustic-structure interface and Neumann boundary. Dirichlet boundary conditions or computations on exterior domains can be implemented without difficulties. On the acoustic-structure interface Γ^{int} the coupling conditions enforce equilibrium $p = f$ and continuity $q = -\rho_0 \omega^2 w$.

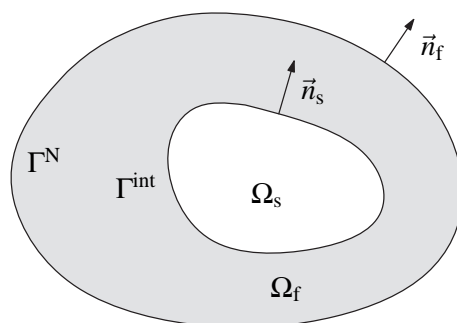


Figure 1: Acoustic-structure interaction

Mortar Coupling

The concept of mortar coupling was introduced by Bernardi *et al.* [1] as a method for non-conforming domain decomposition. In the presented paper, it is formulated for the BEM-FEM simulation of acoustic-structure interaction. The fluid load on the plate is chosen as Lagrange multiplier $\lambda \equiv f^0$, yielding high flexibility in the choice of discretizations.

¹Institut A für Mechanik, Universität Stuttgart, 70550 Stuttgart, Germany

For the Kirchhoff plate a finite element formulation is chosen. Starting point is the bi-linear form given by

$$a(\nabla w, \nabla v) = \int_{\Gamma^{\text{int}}} \left[D(1-\nu) \left(\frac{\partial^2 v}{\partial x_1^2} \frac{\partial^2 w}{\partial x_1^2} + 2 \frac{\partial^2 v}{\partial x_1 \partial x_2} \frac{\partial^2 w}{\partial x_1 \partial x_2} + \frac{\partial^2 v}{\partial x_2^2} \frac{\partial^2 w}{\partial x_2^2} \right) + D\nu \Delta v \Delta w - \rho_s t \omega^2 w v \right] ds_x. \quad (1)$$

The displacement field is given by the solution of

$$a(\nabla w, \nabla v^w) - \int_{\Gamma^{\text{int}}} v^w \lambda ds_x = \int_{\Gamma^{\text{int}}} v^w f^e ds_x. \quad (2)$$

The boundary element method is employed for the acoustic domain. A detailed introduction to the method can be found in [3]. The two basic equations are the boundary integral equation

$$p(x) = \frac{1}{2} p(x) + \underbrace{\int_{\Gamma} P^*(x,y) q(y) ds_y}_{(Vq)(x)} - \underbrace{\int_{\Gamma} \frac{\partial P^*(x,y)}{\partial n_y} p(y) ds_y}_{(Kp)(x)}, \quad x \in \Gamma, \quad (3)$$

and the hyper-singular boundary integral equation

$$q(x) = \frac{1}{2} q(x) + \underbrace{\int_{\Gamma} \frac{\partial P^*(x,y)}{\partial n_x} q(y) ds_y}_{(K'q)(x)} - \underbrace{\int_{\Gamma} \frac{\partial^2 P^*(x,y)}{\partial n_x \partial n_y} p(y) ds_y}_{-(Dp)(x)}, \quad x \in \Gamma. \quad (4)$$

The single layer potential $(Vq)(x)$, double layer potential $(Kp)(x)$, adjoint double layer potential $(K'q)(x)$ and the hyper-singular operator $(Dp)(x)$ are the well-known boundary integral operators with the fundamental solution $P^*(x,y) = e^{i\kappa|x-y|}/(4\pi|x-y|)$ defining the integration kernels.

For the coupling algorithm, the pressure and flux fields on the boundary are decomposed: $p = p^{\text{int}} + \tilde{p}$ and $q = q^{\text{int}} + \tilde{q}$, where \tilde{q} are the prescribed Neumann boundary conditions and $p^{\text{int}} = q^{\text{int}} = 0$ on Γ^{N} .

Using Eq. (3) tested with v^q on Γ^{int} and Eq. (4) tested with v^p on the entire boundary Γ one obtains the system

$$\int_{\Gamma^{\text{int}}} v^q (Vq^{\text{int}})(x) ds_x + \int_{\Gamma^{\text{int}}} v^q \left[-\frac{1}{2} p^{\text{int}}(x) - (Kp^{\text{int}})(x) \right] ds_x - \int_{\Gamma^{\text{int}}} v^q (K\tilde{p})(x) ds_x + \int_{\Gamma^{\text{int}}} v^q \left[p^{\text{int}}(x) - \lambda(x) \right] ds_x = - \int_{\Gamma^{\text{int}}} v^q (V\tilde{q})(x) ds_x, \quad (5)$$

$$\int_{\Gamma} v^p (Dp^{\text{int}})(x) ds_x + \int_{\Gamma} v^p (D\tilde{p})(x) ds_x + \int_{\Gamma} v^p \left[-\frac{1}{2} q^{\text{int}}(x) + (K'q^{\text{int}})(x) \right] ds_x = \int_{\Gamma} v^p \left[\frac{1}{2} \tilde{q}(x) - (K'\tilde{q})(x) \right] ds_x. \quad (6)$$

The term $p^{\text{int}}(x) - \lambda(x)$ in Eq. (5) was introduced to enforce equilibrium on the interface. Continuity is enforced by

$$\int_{\Gamma^{\text{int}}} v^\lambda (\rho_0 \omega^2 w + q^{\text{int}}) ds_x = 0. \quad (7)$$

The shape functions and nodal vectors of the discretization are defined as follows

$$\begin{aligned} w_h(x) &= \boldsymbol{\varphi}^w(x) \mathbf{w}, & \lambda_h(x) &= \boldsymbol{\varphi}^\lambda(x) \lambda, \\ q_h^{\text{int}}(x) &= \boldsymbol{\varphi}^q(x) \mathbf{q}^{\text{int}}, & p_h^{\text{int}}(x) &= \boldsymbol{\varphi}^p(x) \mathbf{p}^{\text{int}}, & \tilde{p}_h(x) &= \boldsymbol{\varphi}^p(x) \tilde{\mathbf{p}}. \end{aligned} \quad (8)$$

For the Kirchhoff plate, the ansatz functions must fulfill C^1 continuity requirements. Incomplete bi-cubic polynomials are used on rectangular elements. The element has 12 degrees of freedom: one displacement and two rotation coordinates at each node. The acoustic pressure is discretized with linear ansatz functions on triangles whereas the acoustic flux is discretized with constant ansatz functions on triangles. The Lagrange multiplier is discretized on Γ^{int} using the boundary element mesh with linear ansatz functions. On the edges of Γ^{int} the ansatz space of the Lagrange multiplier is restricted to constant functions in order to fulfill the inf-sup condition of the resulting saddle point problem. A two dimensional illustration of the modification is shown in Fig. 2.

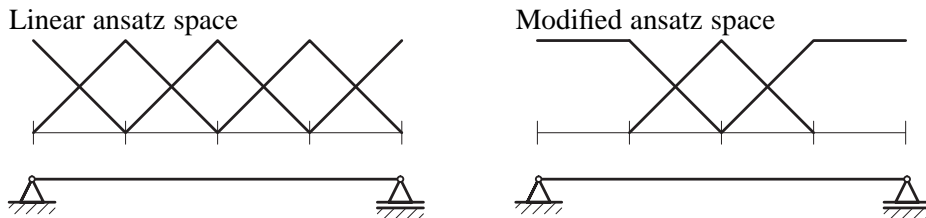


Figure 2: Modification of the ansatz space for the Lagrange multiplier

Combining the discretized plate equation (2), fluid equations (5), (6) and continuity equation (7), one obtains the system of equations

$$\begin{pmatrix} \rho_0 \omega^2 \mathbf{A} & \mathbf{0} & \mathbf{0} & \mathbf{0} & -\mathbf{C}_{\text{FEM}} \\ \mathbf{0} & \mathbf{V} & \frac{1}{2} \mathbf{M} - \mathbf{K}_{\text{int,int}} & -\mathbf{K}_{\text{int,N}} & -\mathbf{C}_{\text{BEM}} \\ \mathbf{0} & -\frac{1}{2} \mathbf{M}^T + \mathbf{K}_{\text{int,int}}^T & \mathbf{D}_{\text{int,int}} & \mathbf{D}_{\text{int,N}} & \mathbf{0} \\ \mathbf{0} & \mathbf{K}_{\text{N,int}} & \mathbf{D}_{\text{N,int}} & \mathbf{D}_{\text{N,N}} & \mathbf{0} \\ \mathbf{C}_{\text{FEM}}^T & \mathbf{C}_{\text{BEM}}^T & \mathbf{0} & \mathbf{0} & \mathbf{0} \end{pmatrix} \begin{pmatrix} \mathbf{w} \\ \mathbf{q}^{\text{int}} \\ \mathbf{p}^{\text{int}} \\ \tilde{\mathbf{p}} \\ \lambda \end{pmatrix} = \begin{pmatrix} \rho_0 \omega^2 \int_{\Gamma^{\text{int}}} \boldsymbol{\varphi}^w f^e ds_x \\ - \int_{\Gamma^{\text{int}}} \boldsymbol{\varphi}^q (V \tilde{q})(x) ds_x \\ \int_{\Gamma} \boldsymbol{\varphi}^p [\frac{1}{2} \tilde{q}(x) - (K^l \tilde{q})(x)] ds_x \\ \mathbf{0} \end{pmatrix}. \quad (9)$$

For the solution of the system (9) an approximate Uzawa type algorithm is employed. GMRES iterations are performed on the reduced equation for the Lagrange multiplier λ . The inverse of the FEM matrix is approximated by conjugate gradient iterations, while the BEM Dirichlet-Neumann map for the acoustic domain is evaluated using inner GMRES iterations.

In the approximate Uzawa algorithm, matrix-vector products of discretized boundary integral operators must be evaluated. Using a standard BEM formulation, the computing time and memory requirements are of order $O(N^2)$ and the method is thus not feasible for large scale simulations. Using the fast multipole BEM, the numerical cost can be reduced to $O(N \log^2 N)$. For a description of the multipole algorithm it is referred to a paper by the authors [2].

Numerical Example

The proposed coupling algorithm is demonstrated on the example of an acoustic cavity backed by an elastic panel. For this model problem, an analytic series solution was developed by Pretlove [4] that is used as a reference solution. The elastic panel considered has the dimensions $1\text{ m} \times 1\text{ m}$ and a thickness of $t = 0.01\text{ m}$. It is made from steel ($E = 2.1 \times 10^{11}\text{ N/m}^2$, $\nu = 0.3$, $\rho = 7900\text{ kg/m}^3$) and is simply supported on all edges. The panel is coupled to a closed acoustic cavity with dimensions $1\text{ m} \times 1\text{ m} \times 1\text{ m}$. The remaining surfaces of the cavity are reverberant walls, i.e. homogeneous Neumann boundary conditions ($\bar{q} = 0$) are applied. The acoustic fluid is water ($c_0 = 1481\text{ m/s}$, $\rho = 1000\text{ kg/m}^3$).

Fig. 3 plots the frequency response at the point $(0.2\text{ m}, 0.3\text{ m})$ on the plate due to a force of $F = 1\text{ N}$ at the same position. The FEM-BEM results computed using 8 boundary elements per edge and 20×20 finite plate elements agree completely with the series solution.

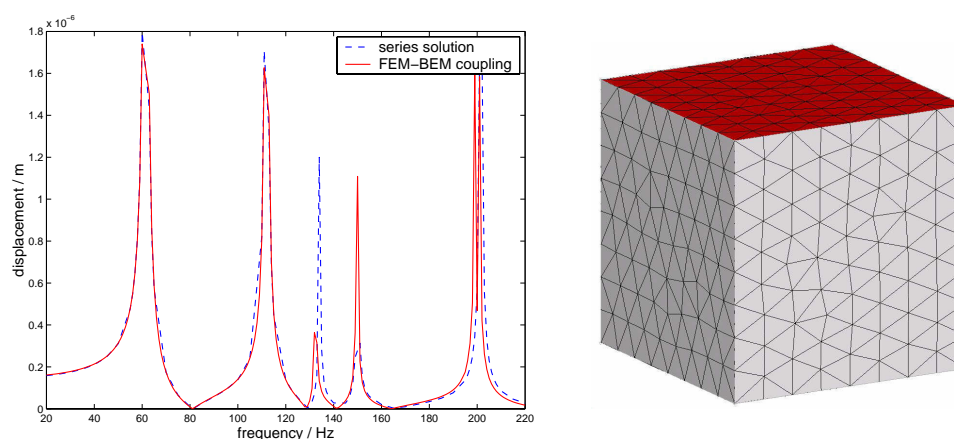


Figure 3: Frequency response of plate coupled to acoustic cavity and BEM model used for the computation.

The vibration modes of the plate close to the resonance peaks are shown in Fig. 4. Comparing the vibration modes to the eigenmodes of an uncoupled plate, the effect of the acoustic cavity is particularly noticeable for mode shapes that have a non-zero average flux over the interface. Then, the stiffness effect of the cavity plays a dominant role. For example, the first uncoupled eigenfrequency of the plate is found at 49Hz whereas its mode shape can be identified at a frequency of 132Hz for the coupled system. Mode shapes with zero average flux are found at frequencies slightly below their uncoupled counterparts due to the added mass effect.

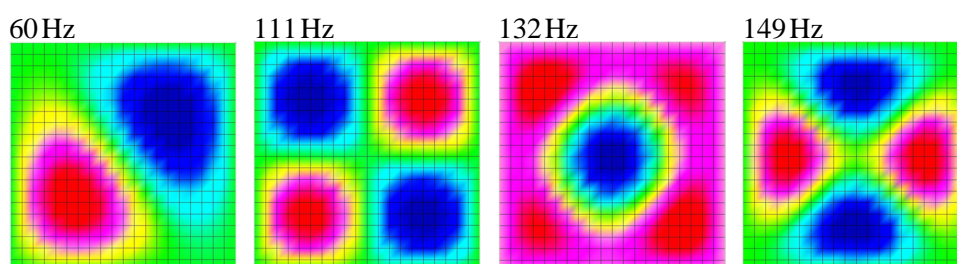


Figure 4: Vibration modes of plate.

To demonstrate the flexibility of the algorithm with respect to mesh refinement in the sub-domains, the system is studied at a frequency of $f = 180\text{Hz}$ with forcing by a single force as before. The resulting displacement field is depicted in Fig. 5. The errors of the displacement and pressure fields on the interface are defined as

$$e_2^{\text{structure}} = \frac{\|\mathbf{w}_{\text{FEM}} - \mathbf{w}_{\text{series}}\|_2}{\|\mathbf{w}_{\text{series}}\|_2} \quad \text{and} \quad e_2^{\text{fluid}} = \frac{\|\mathbf{p}_{\text{BEM}}^{\text{int}} - \mathbf{p}_{\text{series}}^{\text{int}}\|_2}{\|\mathbf{p}_{\text{series}}^{\text{int}}\|_2}, \quad (10)$$

respectively. In Tab. 1 the errors are shown for refined FEM and BEM meshes. A rather fine FEM discretization is required for the spatial resolution of the displacement field. Thus, the errors reduce quickly with FE mesh refinement until the maximum accuracy for the chosen fluid mesh is obtained (see Fig. 5).

Furthermore, Tab. 1 shows the required GMRES iterations on the reduced equation. The iteration count increases moderately with refinement of the boundary element mesh, i.e. refinement of the Lagrange multiplier mesh. The FEM and BEM sub-systems are, so far, scaled using standard diagonal preconditioning, thus, offering significant potential for improvement of the algorithm.

Reference

1. Bernardi, C., Maday, Y., and A.T. Patera (1994): "A new nonconforming approach to domain decomposition: the mortar element method", in Brezis, H., *et al.* (eds.): *Nonlinear Partial Differential Equations and their Applications*, Pitman, pp. 13-51.

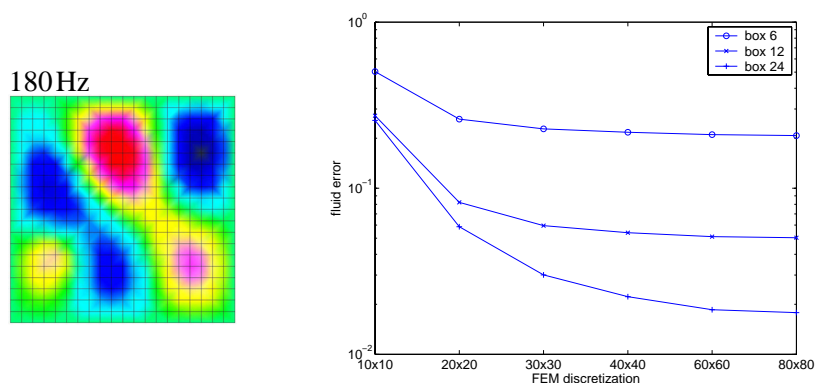


Figure 5: Displacement field and fluid error e_2^{fluid} at 180Hz

2. Fischer, M., Gauger, U., and Gaul, L. (2004): “A multipole Galerkin boundary element method for acoustics”, *Engineering Analysis with Boundary Elements*, Vol. 28, pp. 155-162.
3. Gaul, L, Kögl, M., and Wagner, M. (2003): *Boundary Element Methods for Engineers and Scientists*, Springer.
4. Pretlove, A.J (1966): “Forced vibrations of a rectangular panel backed by a closed rectangular cavity”, *Journal of Sound and Vibration*, Vol. 3(3), pp. 252-261.

Table 1: Error of displacement and pressure field on the interface at 180Hz.

		iterations	$e_2^{\text{structure}}$	e_2^{fluid}
box 6 (144 elements on interface)	plate 10×10	31	42.05%	50.39%
	plate 20×20	31	14.36%	26.06%
	plate 40×40	31	8.75%	21.73%
	plate 80×80	31	7.40%	20.75%
box 12 (576 elements on interface)	plate 10×10	45	29.58%	27.33%
	plate 20×20	46	6.63%	8.23%
	plate 40×40	46	1.82%	5.40%
	plate 80×80	46	0.68%	5.03%
box 24 (2304 elements on interface)	plate 10×10	75	29.10%	25.61%
	plate 20×20	77	6.31%	5.87%
	plate 40×40	78	1.53%	2.22%
	plate 80×80	79	0.43%	1.78%